Influence of surface tension changes on hydrodynamic flow induced by traveling chemical waves

Kai Matthiessen,[1] Hermann Wilke,[2] and Stefan C. Müller[1,*]
[1]*Max-Planck-Institut für molekulare Physiologie, Rheinlanddamm 201, 44139 Dortmund, Germany*
[2]*Institut für Theoretische Physik, Technische Universität Berlin, Rudower Chaussee 5, Geb. 2.14, D-12489 Berlin, Germany*
(Received 12 February 1996)

Chemical waves in a thin layer of a Belousov-Zhabotinsky reaction solution induce convective flow in the reaction medium. The mechanism of this chemically driven convection is investigated with space-resolved velocimetry, and simulated numerically solving modified Oregonator model equations and the Navier-Stokes equation. To decide whether the flow is driven by surface tension gradients or density gradients the results of the simulations are compared with experimental data. Analysis of the vertical distribution of the horizontal flow velocity suggests that in the mechanism of flow generation surface effects are dominant. [S1063-651X(96)07206-6]

PACS number(s): 47.70.Fw, 47.20.Dr, 47.20.Bp, 82.20.Wt

I. INTRODUCTION

During the last 25 years the Belousov-Zhabotinsky (BZ) reaction has evolved to one of the most established systems for the investigation of chemical waves in an excitable medium [1,2]. The spatiotemporal behavior of circular and spiral waves in a thin layer of BZ solution was examined intensively as a function of various external parameters. It has now become common to investigate the reaction in a gel matrix to avoid the influence of hydrodynamic disturbances. Especially in continuously fed open reactors, gels are indispensable to avoid pattern deformation due to the inflow and outflow of the reactants.

On the other hand, convective phenomena in the BZ reaction have become an interesting object to study the coupling between a pattern forming chemical reaction and hydrodynamic motion. The reaction produces changes of species concentrations and temperature and therefore affects the density and surface tension of the reaction solution [2–5]. If it is performed in a liquid solution without a gel, these changes can give rise to convective flow patterns traveling along with the chemical waves [6]. This type of chemically driven convection provides a transport mechanism additional to the diffusion. From the hydrodynamic point of view, the chemical waves represent an external forcing of a complex fluid.

Several authors have investigated the phenomenon of convection driven by chemical waves experimentally [6–9]. A horizontal layer of BZ solution of less than 1-mm thickness in a covered Petri dish is a commonly used arrangement to examine this type of convection. The hydrodynamic flow can be measured by the observation of small suspended tracer particles [10]. The measurements show that the flow behavior depends on the wavelength of the chemical waves. With large wavelengths, as they typically appear in a circular wave pattern, individual pairs of convection rolls with a pronounced descending flow near the front are observed [6]. A short wavelength leads to a complex cooperative flow behavior that is extended over several (in the order of ten) chemical fronts [9,10]. This flow normally occurs in a spiral wave pattern which typically has a short wavelength.

Different computer models have been used to study the basic flow field in a vertical cut through the thin layer on the basis of a simplified reaction-diffusion mechanism [11–15]. In all of these models the convection was coupled to the chemical reaction assuming density changes of the reaction medium due to the chemical oscillation. In this study we will focus our attention in addition on surface tension gradients, generated by the concentration of different chemical species as the driving force. Although measurements of Yoshikawa *et al.* show a clear influence of the proceeding BZ reaction on the surface tension [16], no simulations have yet been done to model this coupling mechanism. Temperature effects are not considered because they do not play a significant role in this type of chemically driven convection [17].

The two conceivable types of hydrodynamic interactions are the Marangoni-type convection induced by surface tension gradients, and the Rayleigh-Bénard-type convection driven by density gradients in the bulk [5]. In several numerical simulations it was pointed out that it is indeed possible to obtain flow fields which appear very similar to the observed fields by only assuming density gradients generated by the chemical reaction as the driving force [14,15]. Pojman and Epstein were able to estimate the magnitude of the induced density differences just by using values from the literature for the different hydration of the oxidized and the reduced form of the catalyst ferroin [5]. We intend to clarify whether the Marangoni-type convection leads to an even better agreement with the experiments.

The easiest way to check the role of Marangoni-type convection experimentally in the chemically driven convection is to eliminate the free surface with a cover placed directly on the fluid layer. However, because of the gas production of the BZ reaction this procedure give rise to serious experimental problems, as the system will become disturbed by bubbles. Since also no direct measurement of the reaction-induced density changes is yet available, we chose an indirect way to decide between the influence of surface and bulk effects. We simulated the induced flow for both types of

*Permanent address: Institut für Experimentelle Physik, Otto-von-Guericke-Universität-Magdeburg, Abteilung Biophysik, Universitätsplatz 2, D-39106 Magdeburg, Germany.

convection numerically for a single horizontally moving pulse, and compared the vertical distribution of the horizontal flow velocity for each case with the experimental results. For this purpose we present some numerical results solving the complete set of time-dependent PDE's of the model using a finite-element method [14]. The presented experimental flow profile is the result of several complete flow velocity experiments for each of ten different heights. As the main result, the comparison of the flow distributions indicates that the Marangoni-type convection is dominant in chemically driven convection in the Belousov-Zhabotinsky reaction.

II. NUMERICAL METHODS AND RESULTS

The numerical problem is intrinsically a three-dimensional one, because the experimental fluid layer is extended in all three spatial dimensions [6]. In particular the height, which is often neglected in convection-free systems, must be included for the hydrodynamic motion. According to the experiments we restrict our considerations to the so-called target patterns which consist of concentric rings of traveling waves with a large wavelength on the order of 10 mm [6]. If the waves are triggered in the middle of the circular Petri dish, the spatial wave propagation can be taken as two dimensional in a vertical cut due to the rotational symmetry.

For the modeling convective terms have to be added to the currently used ''Oregonator'' model which describes the interaction of reaction and diffusion in excitable media [2,14]. In addition, the time-dependent Navier-Stokes equations have to be solved in two spatial dimensions. To introduce the conceivable effects of chemical concentration gradients on the convection, buoyancy as well as surface tension σ must be taken into account. As already presented in Ref. [14], the buoyancy forces induced by the concentrations of the activator (c_1) and the inhibitor (c_2) appearing in the Oregonator model are represented by the Grashof numbers Gr_1 and Gr_2, respectively (see below). To include changes in the surface tension induced by concentration differences, the stress-free boundary condition at the surface is replaced by the equilibrium of tangential stress,

$$\mu\frac{\partial u}{\partial y}=\zeta_i\frac{\partial c_i}{\partial x} \quad \text{where} \quad \zeta_i=\left|\frac{d\sigma}{dc}\right|_i=\text{const}, \quad \text{and} \quad i=1,\ 2.$$

The flow velocities are u in the horizontal direction and v in the vertical direction. The concentration c_1 of the activator and c_2 of the inhibitor are functions of the Cartesian coordinates x (length), y (height), and time t. The dynamic viscosity μ is a property of the liquid. The dependence of the surface tension σ_i on the concentrations of species i is assumed to be linear. For the set of the partial differential equations (PDE's) and boundary conditions we refer to [14], using a rectangular domain of length L and depth H with a symmetry line at the left side (center of the circular Petri dish), rigid walls at the right side and at the bottom and a plane-free upper surface, which is not deformed by the convection. Using the Oregonator length unit $x_0=0.18$ mm and time unit $t_0=21$ s [18] for scaling, the numerical solution of the problem depends only on the following dimensionless parameters:

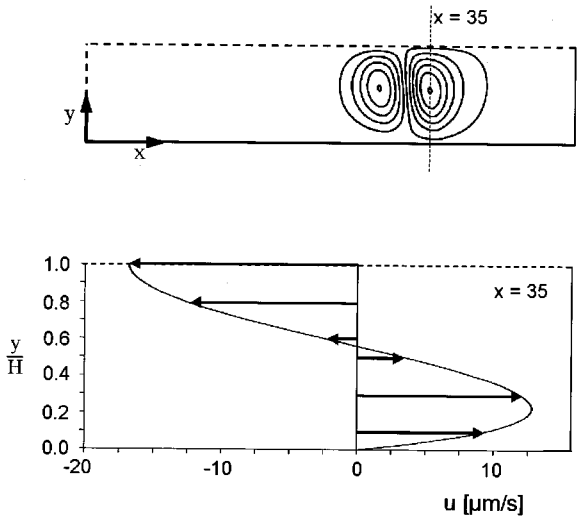

FIG. 1. Streamlines and corresponding distribution of the horizontal velocity for the buoyancy-driven case linked to the activator ($\mathrm{Gr}_1=0.01$). At the dimensionless position $x=35$ the front reached a stationary state of propagation.

$$\mathrm{Gr}_i=\frac{g\dfrac{\delta\rho_i}{\rho_i}x_0^3}{\nu^2}, \quad \mathrm{Ma}_i=\frac{\zeta_i c_0 x_0}{\mu\nu}, \quad D_i=\frac{d_i t_0}{x_0^2}, \quad D_\nu=\frac{\nu t_0}{x_0^2},$$

where $i=1$ and 2.

Gr_i represents the Grashof numbers, Ma_i represents the Marangoni numbers, and D_i and D_ν represent the dimensionless diffusion coefficients of the species and momentum, respectively. In the equations d_i are the diffusion coefficients of the activator (1) and the inhibitor (2), ν the kinematic viscosity, g the gravitational acceleration, and ρ the density. Dividing D_ν by D_i, one obtains the often used Schmidt number Sc_i. The values of $\mathrm{Gr}_{1,2}$ and $\mathrm{Ma}_{1,2}$ represent the four possible types of hydrodynamic coupling: density- or surface-tension-driven convection coupled to the concentration of the activator or the inhibitor, respectively. The obtained set of PDE's was solved numerically using the ENTWIFE computer code [19]. A graded mesh of mixed finite elements was carefully designed in order to obtain a sufficiently accurate approximation of the solution (for details, see [14].) The numerical effort for the Marangoni case is higher as compared to the buoyancy driven convection, because steep velocity gradients located near the free upper surface require a finer mesh.

To show the influence of convective interactions concerning the different types of coupling, a large number of numerical experiments were performed. During the calculations the following parameters remain unchanged: $D_1=1.0$, $D_2=0.6$, and $D_\nu=600$; the Oregonator parameters $\epsilon=0.01$, $f=2.0$, and $q=0.002$ [18], and the system dimensions. $L=50x_0$ and $H=5x_0$. We consider ''clean'' interactions, which means that only one of the four coupling parameters Gr_1, Gr_2, Ma_1, or Ma_2 is set to a nonzero value.

In Fig. 1 a snapshot of the moving fluid for $\mathrm{Gr}_1=0.01$ is presented, showing streamlines of the flow field, representing a buoyancy driven convection linked to the activator concen-

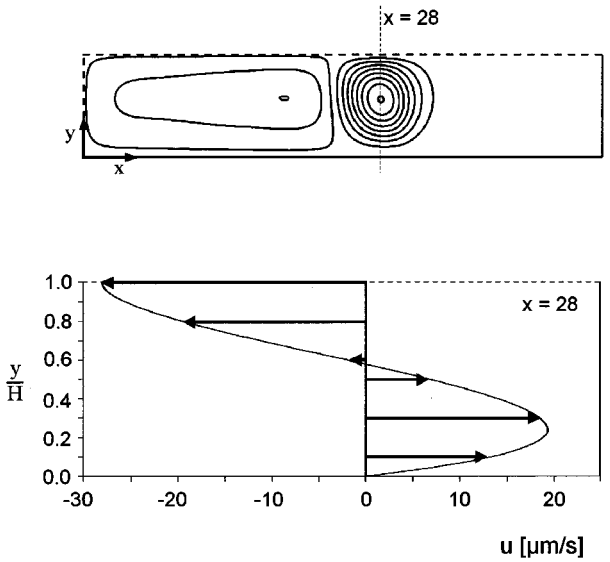

FIG. 2. Streamlines and corresponding distribution of the horizontal velocity for the buoyancy-driven case linked to the inhibitor ($Gr_2 = 0.02$).

tration. The lower part of Fig. 1 shows the corresponding horizontal flow velocity distribution along the vertical direction at a position which is selected for comparison with experiments. The pulse was started at the symmetry line $x = 0$ and moved to the location indicated by the two vortices shown in Fig. 1 during the calculation. It turns out that a strong fluid motion evolves only in the vicinity of the pulse position. This is a consequence of the nearly symmetric sharp concentration gradients at the ascending and descending part of the activator pulse. The horizontal flow velocity below shows the typical shape of a buoyancy driven convection with zero velocity near the half height of the solution layer (at $y/H \approx 0.6$). Figure 2 was obtained for $Gr_2 = 0.02$, representing a buoyancy-driven convection linked to the inhibitor concentration. It shows a similar scenario but with a pronounced ''tail'' of the vortex behind the wave. The specific Grashof numbers $Gr_{1,2}$ were chosen to obtain surface velocities comparable to the experimentally observed ones. Additional simulations have shown that the velocity height profiles remain isomorphic for a larger interval of Grashof numbers.

We now turn to surface-tension-driven convection, which is characterized by a focusing of streamlines near the surface. The results shown in Fig. 3 were calculated with $Ma_1 = 0.05$ representing the case of Marangoni-type convection linked to the activator concentration. The calculation yields a maximum velocity of about 26 μm/s. The corresponding profile for the horizontal velocity differs considerably from the buoyancy-driven case. The position of zero velocity is shifted to the upper system boundary, indicating as expected that the convection is driven by forces at the surface. Finally, in Fig. 4 the results for Marangoni-type convection linked to the inhibitor concentration via $Ma_2 = 0.5$ are presented. Although the maximum horizontal velocity is of the same order of magnitude as in Fig. 3, the streamlines appear to be quite different. The asymmetric shape of the inhibitor concentration in a pulse produces only one strong vortex like in the density-driven case. The other

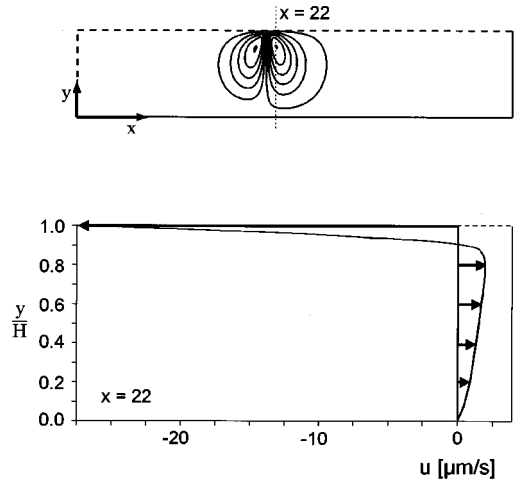

FIG. 3. Streamlines and corresponding distribution of the horizontal velocity for the surface-tension-driven case linked to the activator ($Ma_1 = 0.05$).

vortex behind the wave seems to be driven only by the strong one in front of the wave. The height where the flow changes its direction is, in this case, only slightly shifted toward the surface.

III. EXPERIMENTAL PREPARATIONS AND RESULTS

Experiments were performed with a commonly used BZ recipe. The initial concentrations were (disregarding the bromination of ferroin [18]). 340-m*M* $NaBrO_3$, 48-mM NaBr, 96-mM malonic acid, 380-mM sulfuric acid, and 3.5-mM ferroin. For the flow measurements 4 ml of the solution are filled into a specially cleaned Petri dish. A careful cleaning procedure is necessary to avoid the generation of gas bubbles

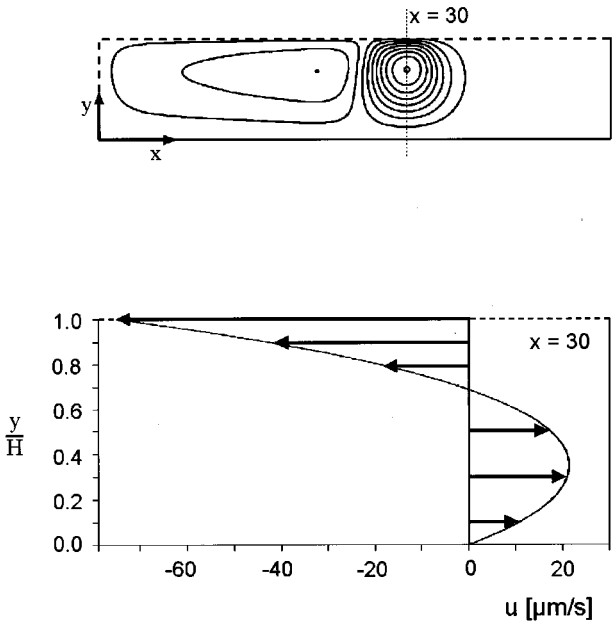

FIG. 4. Streamlines and corresponding distribution of the horizontal velocity for the surface-tension-driven case linked to the inhibitor ($Ma_2 = 0.5$).

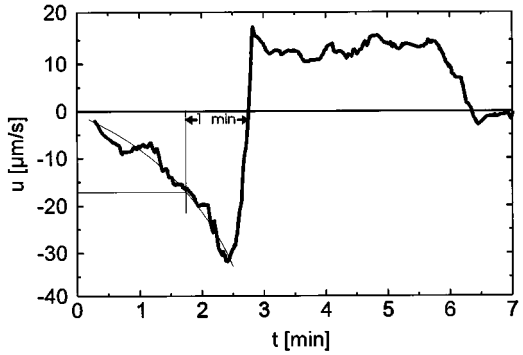

FIG. 5. Experimentally obtained flow velocity at the surface of the fluid layer as a function of time. The chemical wave was generated in the center of the dish, and the flow was measured half the way to the boundary.

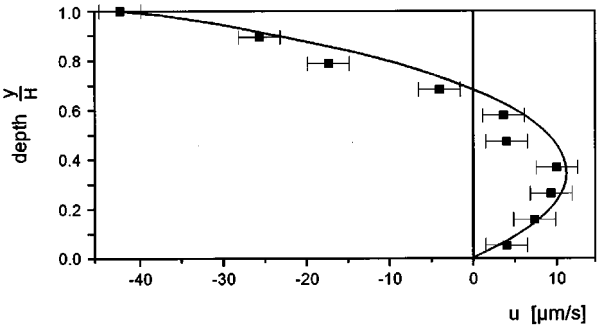

FIG. 6. Experimentally obtained vertical profile of the horizontal flow velocity distribution. The curve is fitted from the inhibitor concentration linked Marangoni-type case (Fig. 4) using the total flow amplitude as the free fitting parameter.

and the spontaneous initiation of chemical waves [7]. The solution forms a shallow fluid layer with a thickness of 850 μm in the central region of the Petri dish.

The experimental setup has been described previously [10]. To observe the hydrodynamic motion, small latex particles (Serva, Standard Dow Latex, $\emptyset 0.552 \pm 0.0104$ μm) are suspended in the solution [10]. They scatter the light of a He-Ne laser beam focused on the measuring point. The scattered light is observed by a vidicon camera mounted onto an inverted microscope (Zeiss Im35). Due to the large magnification the depth of focus is small enough to resolve about 30 different planes in the solution layer just by changing the focal plane of the microscope. The video camera images depict a volume of the layer with the side lengths of 400×400 μm^2, and a height of 25 μm in the vertical direction. They are stored on a videotape with at time lapse recorder (Sony Watchcorder) and digitized on a personal computer with a frame grabber card (Data Translation DT2851). From the digitized images of the moving particles the flow velocity can be calculated automatically using the spatial filtering method [9].

A typical flow measurement is shown in Fig. 5. To obtain rotationally symmetric conditions, a circular wave was initiated in the middle of the Petri dish with a silver wire. The flow velocities were measured at a fixed point halfway between center and boundary and at the surface of the fluid layer. The results show an increasing flow velocity, while the front approaches the measuring point. During the passage there is a rapid change in the flow direction. In the back of the wave the flow velocity remains nearly constant until the wave disappears at the dish boundary. Other measurements that are not presented here show, in principle, the same flow behavior near the bottom but in the opposite direction [6]. The results correspond to a pair of convection rolls with a pronounced descending flow in the wave front, traveling with the wave through the medium.

For a comparison of the experimental data with the numerical calculations, the vertical distribution of the horizontal flow velocity has to be measured. With the available experimental setup it is not possible to investigate the flow velocity simultaneously at different heights. Hence we had to obtain the velocity of each height from a separate experiment performed under identical conditions. The experiments are synchronized with the zero transition point of the velocity in the wave front. To minimize the statistical error of the system preparation, several measurements for each height were performed and averaged. Figure 6 shows the horizontal flow velocity 1 min before the front passed the measuring point for ten different heights. The measurement corresponds to a vertical cut through the first convection roll 6.5 mm away from the front.

IV. DISCUSSION

The flow velocity shown in Fig. 5 already indicates that the observed flow phenomena are driven by the concentration of a reaction component that has a sharp rise in the wave front and a smooth decay behind. The strong concentration gradient in the front induces a high flow velocity with a short spatial extent in front of the wave. The weak gradient in the tail produces a spatially extended flow with a lower velocity. In the BZ reaction the catalyst ferroin shows this behavior. In previous publications the ferroin was already postulated to be responsible for the induction of density gradients [5] as well as for surface tension changes [16].

A comparison between the experimental data of Fig. 6 and the buoyancy-driven convection in Figs. 1 and 2 shows great differences in the shape of the flow distribution. In the calculated flow profile there is a much greater similarity between the forward flow part and the back flow part than in the experimental data. Furthermore the surface flow velocity is much too small in relation to the other velocities. On the other hand, the surface-tension-driven flow profile that is linked to the activator concentration (Fig. 3) is much more surface dominated than the experimental distribution. The Marangoni-type convection linked to the inhibitor concentration with $Ma_2 > 0$ (Fig. 4) yields the best fit of the experimental data. The curve in Fig. 6 belongs to this calculation using the total flow amplitude as a free fitting parameter. As additional calculations have shown, this fitting procedure is reasonable as the velocity curve remains isomorphic for a large range of Marangoni numbers and just changes its amplitude. Using this amplitude, we calculated the Marangoni number of the experimental system. On the base of the Oregonator Model we obtain a value of about 0.3 for Ma_2.

Looking more precisely where the data of Fig. 6 are fitting well and where not, in particular the position of zero velocity differs between measurement and calculation. This

is probably an error of the measurement, as an optimal fit of the experimental data would violate the continuity condition because the total integral over the flow velocity would not vanish in this case. However, the difference between fit and data can also indicate that for the given BZ recipe a combination of the surface tension and the buoyancy mechanism may be responsible for the convection. Taking into account a small amount of Rayleigh-type convection would shift the location of zero velocity of the numerical curve closer to the experimental data. We can emphasize this tendency by comparing the surface velocities of the experimental (Fig. 5) and numerical results. The surface velocities in front of the pulse are in good agreement, whereas the numerical velocities behind it are by a factor of 2 too small. This also could be achieved by considering a certain amount of buoyancy-driven convection in the velocity distribution.

At least for the generation of the obtained convection phenomena in the Belousov-Zhabotinsky reaction, surface tension effects are dominant. The hydrodynamic flow generation is linked to the concentration of a chemical component that shows a temporal evolution like the inhibitor. In the Oregonator model the inhibitor represents the concentration of the oxidized catalyst ferroin. That is in a good agreement to the suggestion of Yoshikawa *et al.* [16] that the ferroin concentration differences are the cause of the surface tension gradients in the BZ reaction.

ACKNOWLEDGMENTS

This work was supported by the Deutsche Forschungsgemeinschaft and the Verein der Chemischen Industrie e. V. We thank M. Böckmann and V. Zykov for helpful discussions.

[1] *Chemical Waves and Patterns*, edited by R. Kapral and K. Showalter (Kluwer, Dordrecht, 1994).
[2] *Oscillations and Traveling Waves in Chemical Systems*, edited by R. J. Field and M. Burger (Wiley, New York, 1985).
[3] I. R. Epstein, M. Morgan, C. Steel, and O. Valdés-Aguilera, J. Phys. Chem. **87**, 3955 (1983).
[4] Z. Nagy-Ungvarai, S. C. Müller, J. Tyson, and B. Hess, J. Phys. Chem. **93**, 2760 (1989).
[5] J. A. Pojman and I. R. Epstein, J. Phys. Chem. **94**, 4966 (1990).
[6] H. Miike, S. C. Müller, and B. Hess, Phys. Lett. A **141**, 25 (1989).
[7] H. Miike and S. C. Müller, Chaos **3**, 21 (1993).
[8] H. Miike, H. Yamamoto, S. Kai, and S. C. Müller, Phys. Rev. E **48**, 1627 (1993).
[9] K. Matthiessen and S. C. Müller, Phys. Rev. E **52**, 492 (1995).
[10] H. Miike, S. C. Müller, and B. Hess, Chem. Phys. Lett. **144**, 515 (1988).
[11] Th. Plesser, H. Wilke, and K. H. Winters, Chem. Phys. Lett. **200**, 158 (1992).
[12] J. Masere, D. A. Vasquez, B. F. Edwards, J. W. Wilder, and K. Showalter, J. Phys. Chem. **98** 6505 (1994).
[13] D. A. Vasquez, J. M. Littley, J. W. Wilder, and B. F. Edwards, Phys. Rev. E **50** 280 (1994).
[14] H. Wilke, Physica D **86**, 508 (1995).
[15] Y. Wu, D. A. Vasquez, B. Edwards, and J. W. Wilder, Phys. Rev. E **51**, 1119 (1995).
[16] K. Yoshikawa, T. Kusumi, M. Ukitsu, and S. Nakata, Chem. Phys. Lett. **21**, 211 (1993).
[17] M. Böckmann, B. Hess, and S. C. Müller, Phys. Rev. E **53**, 5498 (1996).
[18] W. Jahnke, W. E. Skaggs, and A. T. Winfree, J. Phys. Chem. **93**, 740 (1989).
[19] K. H. Winters, ENTWIFE, User Manual (Hydrogeology Dept., AEA Technology, Harwell Laboratory, Harwell, 1991).